Crystal structure of the proteasomal deubiquitylation module Rpn8-Rpn11

Ganesh Ramnath Pathare[a], István Nagy[a], Paweł Śledź[a], Daniel J. Anderson[b], Han-Jie Zhou[b], Els Pardon[c,d], Jan Steyaert[c,d], Friedrich Förster[a], Andreas Bracher[e,1], and Wolfgang Baumeister[a,1]

[a]Department of Molecular Structural Biology, Max Planck Institute of Biochemistry, 82152 Martinsried, Germany; [b]Cleave Biosciences, Burlingame, CA 94010; [c]Structural Biology Brussels, Vrije Universiteit Brussel, 1050 Brussels, Belgium; [d]Structural Biology Research Center, Vlaams Instituut voor Biotechnologie, 1050 Brussels, Belgium; and [e]Department of Cellular Biochemistry, Max Planck Institute of Biochemistry, 82152 Martinsried, Germany

Contributed by Wolfgang Baumeister, January 15, 2014 (sent for review December 20, 2013)

The ATP-dependent degradation of polyubiquitylated proteins by the 26S proteasome is essential for the maintenance of proteome stability and the regulation of a plethora of cellular processes. Degradation of substrates is preceded by the removal of polyubiquitin moieties through the isopeptidase activity of the subunit Rpn11. Here we describe three crystal structures of the heterodimer of the Mpr1–Pad1–N-terminal domains of Rpn8 and Rpn11, crystallized as a fusion protein in complex with a nanobody. This fusion protein exhibits modest deubiquitylation activity toward a model substrate. Full activation requires incorporation of Rpn11 into the 26S proteasome and is dependent on ATP hydrolysis, suggesting that substrate processing and polyubiquitin removal are coupled. Based on our structures, we propose that premature activation is prevented by the combined effects of low intrinsic ubiquitin affinity, an insertion segment acting as a physical barrier across the substrate access channel, and a conformationally unstable catalytic loop in Rpn11. The docking of the structure into the proteasome EM density revealed contacts of Rpn11 with ATPase subunits, which likely stabilize the active conformation and boost the affinity for the proximal ubiquitin moiety. The narrow space around the Rpn11 active site at the entrance to the ATPase ring pore is likely to prevent erroneous deubiquitylation of folded proteins.

Mpr1 | POH1 | PSMD7 | PSMD14 | JAMM protease

In eukaryotes, the ubiquitin (Ub) proteasome system (UPS) is responsible for the regulated degradation of proteins (1–5). The UPS plays a key role in the maintenance of protein homeostasis by removing misfolded or damaged proteins, which could impair cellular functions, and by removing proteins whose functions are no longer needed. Consequently, the UPS is critically involved in numerous cellular processes, including cell cycle progression, apoptosis, and DNA damage repair, and malfunctions of the system often result in disease.

The 26S proteasome executes the degradation of substrates that are marked for destruction by the covalent attachment of polyubiquitin chains. It is a molecular machine of 2.5 MDa comprising two subcomplexes, the 20S core particle (CP) and one or two 19S regulatory particles (RPs), which associate with the ends of the cylinder-shaped CP (6–8). The recognition and recruitment of polyubiquitylated substrates, their deubiquitylation, ATP-dependent unfolding, and translocation into the core particle take place in the RP. The structurally and mechanistically well-characterized CP houses the proteolytic activities and sequesters them from the environment, thereby avoiding collateral damage (9).

The RPs attach to the outer α-rings of the CP, which control access to the proteolytic chamber formed by the inner β-subunit rings (10). Recently, the molecular architecture of the 26S holocomplex was established using cryo-EM–based approaches (11, 12), and a pseudoatomic model of the holocomplex was put forward (13). The RP is formed by two subcomplexes, known as the base and the lid, which assemble independently (12, 14). The base contains the hetero-hexameric AAA-ATPase ring (Rpt1–Rpt6), which drives the conformational changes required for substrate processing, including unfolding and translocation into the CP (15, 16). The base also contains the largest RP non-ATPase subunits, Rpn1 and Rpn2, and the Ub receptor Rpn13. The second resident Ub receptor, Rpn10, is not part of either the base or the lid; it binds only to the assembled 26S proteasome and is positioned close to the ATPase module.

The lid scaffold is composed of the Rpn3, Rpn5, Rpn6, Rpn7, Rpn8, Rpn9, Rpn11, and Rpn12 subunits (14). These subunits can be grouped according to their domain structures. Rpn3, Rpn5, Rpn6, Rpn7, Rpn9, and Rpn12 each comprise an N-terminal helix repeat segment, a proteasome-COP9/signalosome-eIF3 (PCI) module, and a long helix at the C terminus (8). The Rpn8 and Rpn11 subunits each consist of an Mpr1–Pad1–N-terminal (MPN) domain, followed by long C-terminal helices (Fig. 1*A*). The PCI subunits form a horseshoe-shaped structure and the MPN domains form a heterodimer, which are connected by a large helical bundle, to which all subunits contribute (13, 17, 18). Each of these eight subunits has paralogs in the COP9/signalosome (CSN) and the elongation initiation factor 3 (eIF3), which likely adopt a similar architecture (18–21).

The lid strengthens the interaction between the CP and RP (17) and deubiquitylates substrates before their processing by the AAA-ATPase module and the CP. Cleavage of polyubiquitin

Significance

The 26S proteasome is a multiprotein complex that degrades proteins marked for destruction by the covalent attachment of polyubiquitin chains. Proteasome activity is essential for the removal of damaged, potentially toxic proteins and for the regulation of numerous cellular processes. Multiple crystal structures of the Rpn8-Rpn11 heterodimer, which is responsible for the removal of polyubiquitin tags before substrate degradation in the proteasome, provide insight into how substrate unfolding and isopeptide bond cleavage might be coupled, and how premature activation of this module is prevented. Its accurate function ensures timely degradation of substrates and, ultimately, the replenishment of the limited cellular pool of free ubiquitin.

Author contributions: G.R.P., I.N., H.-J.Z., F.F., A.B., and W.B. designed research; G.R.P., I.N., P.Ś., D.J.A., and A.B. performed research; E.P. and J.S. contributed new reagents/analytic tools; G.R.P., I.N., P.Ś., D.J.A., F.F., and A.B. analyzed data; and G.R.P., F.F., A.B., and W.B. wrote the paper.

Conflict of interest statement: D.J.A. and H.Z. are full-time employees of Cleave Biosciences.

Freely available online through the PNAS open access option.

Data deposition: The atomic coordinates and structure factors have been deposited in the Protein Data Bank, www.pdb.org (PDB ID codes 4OCL, 4OCM, and 4OCN).

[1]To whom correspondence may be addressed. E-mail: bracher@biochem.mpg.de or baumeist@biochem.mpg.de.

This article contains supporting information online at www.pnas.org/lookup/suppl/doi:10.1073/pnas.1400546111/-/DCSupplemental.

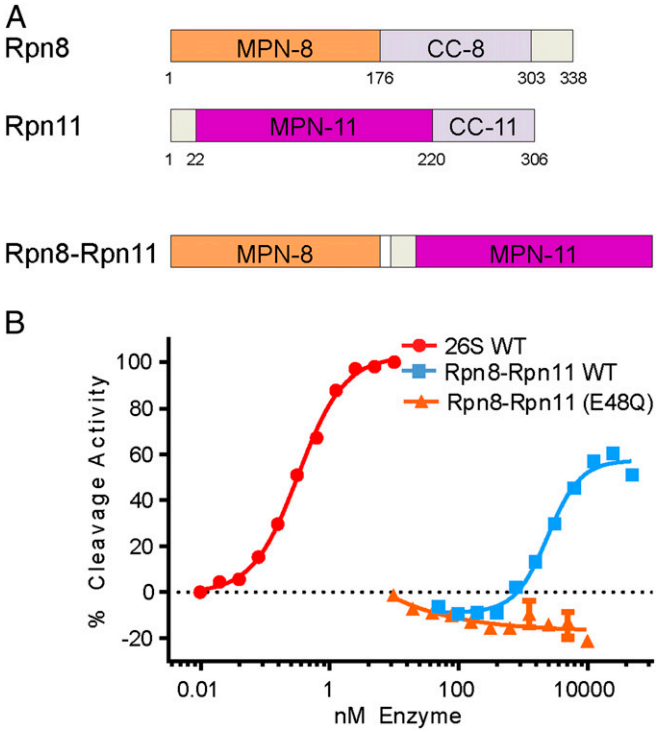

Fig. 1. Biochemical activity of the Rpn8-Rpn11 fusion protein. (*A*) Domain structures of Rpn8, Rpn11 and the fusion protein. (*B*) Ub_4 cleavage activity of 26S proteasome, WT Rpn8-Rpn11 and Rpn8-Rpn11 (E48Q). Cleavage of labeled peptide from Ub_4 was detected by the change in fluorescence polarization after 1hr incubation at 37 °C at the indicated concentrations. Values are normalized to maximum cleavage activity of 26S proteasome. The used 26S proteasome preparation contained only trace amounts of the DUB Ubp6.

chains from the substrate enables recycling of Ub into the cellular pool, and the removal of the unfolding-resistant Ub moieties promotes translocation of substrates. The MPN domain of Rpn11 contains the catalytic site for deubiquitylation (22, 23). Rpn11 belongs to the JAB1/MPN/Mov34 metalloenzyme (JAMM) family of metalloproteases, which provide the isopeptidase activities in the proteasome, CSN, and exo-deubiquitylating enzymes (DUBs), such as associated molecule with the SH3 domain of STAM-like protein (AMSH-LP). The signature motif for this family is a conserved glutamate upstream of a zinc-coordinating catalytic loop, $H(S/T)HX_7SXXD$, first revealed in the structure of an archaeal homolog, AfJAMM (24). The substrate-binding mode of JAMM DUBs was clarified by the crystal structure of AMSH-LP in complex with Lys63-linked diubiquitin (25). The other proteasomal MPN subunit, Rpn8, is catalytically inactive; it does not contain the JAMM motif and appears to have mainly a supporting role for Rpn11. Isolated Rpn11 is catalytically inactive, as is the isolated lid (22). Rpn11 is activated upon integration into the 26S holocomplex and is dependent on ATP hydrolysis (23). The 26S proteasome was recently shown to undergo large-scale conformational changes from a substrate-accepting conformation to a substrate-engaged conformation that may be critical for Rpn11 function (15, 26), but the mechanistic basis for the regulation of Rpn11 remains unclear. Loss-of-function mutants of the JAMM motif cause stalling of substrates above the mouth of the ATPase module and lead to clogging of the 26S proteasome (23, 26).

Inhibitors of human Rpn11 (hRpn11, also known as POH1) have been proposed as potential antitumor agents working upstream of the β5 proteolytic subunits in the UPS. The β5 subunits have been clinically validated by the approval of bortezomib and carilfzomib for the treatment of hematologic malignancies. siRNA and mutagenesis studies show that expression of the zinc catalytic domain of hRpn11 is essential for cell survival (27). Inhibition of hRpn11 in combination with EGFR inhibition has been suggested to be beneficial in the treatment of nonsmall cell lung cancer (28). Overexpression of hRpn11 in cancer cells has been linked to their tumor escape from cytotoxic agents (29). Thus, hRpn11 is an attractive target for pharmacologic intervention of the UPS.

Here we present three crystal structures of the catalytically active Rpn8/Rpn11 MPN heterodimer from *Saccharomyces cerevisiae*, revealing the details of the Rpn11 active site and the mode of interaction with other subunits. Not all structures show proper active site geometry, hinting at possible mechanisms preventing activation outside of the proteasome complex. The access path for the C-terminal peptide of the substrate-bound Ub is blocked by a highly conserved insertion specific to Rpn11. Fitting of the Rpn8-Rpn11 crystal structure into the cryo-EM density of both the substrate-accepting and substrate-engaged proteasome revealed how the subcomplex is situated between base and PCI domain subunits, which involves long insertions unique to Rpn11 and Rpn8. Contacts to the coiled coils and the oligosaccharide-binding fold (OB) domain ring of the AAA subunits appear to control active site geometry and proper access of the isopeptide bond segment. In the substrate-engaged proteasome, the catalytic center becomes situated just above the maw of the ATPase ring.

Results and Discussion

Structure Determination of the Rpn8-Rpn11 Core Complex. The MPN domains of Rpn8 and Rpn11 were expressed as a fusion protein with a 9-aa-long connecting linker (Fig. 1*A*). The domain limits were selected based on limited proteolysis experiments with proteinase K (residues 1–175 of Rpn8 and residues 1–219 of Rpn11), and the domains were fused to ensure stability and formation of a stoichiometric complex. Notably, this fusion construct, designated Rpn8-Rpn11, cleaves a model substrate, a linear tetraubiquitin (Ub_4)-peptide fusion protein, indicating that this construct samples the catalytically active conformation. It requires a 7,000-fold higher concentration than the complete proteasome, however (Fig. 1*B*).

The Rpn8-Rpn11 crystals suitable for structure determination were grown with the aid of a tailored nanobody (variable domain of camelid heavy chain-only antibodies). Rpn8-Rpn11–specific nanobodies were selected from llama antisera raised against purified yeast 26S proteasome. The successful nanobody Nb1 inhibited the deubiquitylation activity of 26 proteasome in a concentration-dependent manner (Fig. S1).

Crystal Lattices. We obtained three crystal forms, here designated Ia, Ib and II, of the Rpn8-Rpn11 fusion protein complex with the nanobody (Table S1 and Fig. S2 *A* and *B*). Crystal forms Ia and Ib are closely related. All crystal forms contain two Rpn8-Rpn11-nanobody complexes per asymmetric unit. The backbones in the core regions of the complex subunits are very similar, yielding rmsd values between 0.304 and 0.916 Å (Fig. S2 *C* and *D*); only helix α4 of Rpn8 is displaced in one copy of crystal form II (Fig. S2*C*). No density could be assigned to any of the linker regions between the Rpn8 and Rpn11 MPN domains.

A major difference between crystal forms I and II is the presence of bound Zn in the former. In crystal form II, a crystal contact between the two copies of Rpn11 distorts the geometry of the catalytic loop, displacing the Zn-coordinating residue His109 from the Zn-binding site (Fig. S2*F*). Thus, crystal form II appears to be incompatible with Zn binding. Thus, we focus on crystal form Ia, diffracting to the highest resolution (2.0 Å).

Structure of the Rpn8-Rpn11 Complex. The Rpn8-Rpn11 core complex structure exhibits pseudo-twofold symmetry (Fig. 2). Each protomer assumes a MPN domain fold and consists of four α-helices, α1–α4, flanking a circular β-sheet of seven β-strands, βA–βG (Figs. S2*E* and S3). The topology of the β-sheet is βA-βC-βB-βD-βE-βF-βG. The long, twisted β-strand βG makes contacts with both βA and βF. Rpn8 and Rpn11 contact each other via two pseudosymmetrical interfaces, a coiled coil between helices α2 and a four-helix bundle of helices α1 and α4 (Fig. 2). The C-terminal α4 helices are associated mainly with the opposing subunit (Fig. 2), causing the domain swapping first observed in the crystal structure of human Rpn8/Mov34 (30) and anticipated in the pseudoatomic models of the 26S proteasome (11, 12).

Two regions connecting βC-α2 and βF-βG are variable in MPN domain sequences, designated here as insertion 1 and insertion 2 (Fig. 2) (24, 25, 30–32). Insertion 1 of Rpn8 forms a β-hairpin on top of the MPN domain. The corresponding region in Rpn11 forms a poorly ordered loop adjacent to the active site, as discussed in more detail below. The insertion 2 regions of Rpn8 and Rpn11 protrude from the opposite ends of the pseudo-twofold symmetric subcomplex (Fig. 2). Insertion 2 of Rpn8 assumes an elongated β-hairpin structure in crystal form II. The hairpins from two Rpn8 molecules align to create a mixed β-sheet contact in this crystal lattice (Fig. S2*B*). In the form I crystal structures, the tips of the β-hairpin are disordered, suggesting that this region is stably structured only in the presence of a suitable interaction partner. The much longer insertion 2 in Rpn11 forms a helical protrusion with a disordered tip in crystal forms Ia and Ib. The helices from two adjacent Rpn11 molecules form antiparallel three-helix bundles (Figs. S2*A* and S3). In crystal form II, both corresponding segments are disordered, suggesting that insertion 2 of Rpn11 stably folds only in appropriate environments, in line with secondary structure predictions.

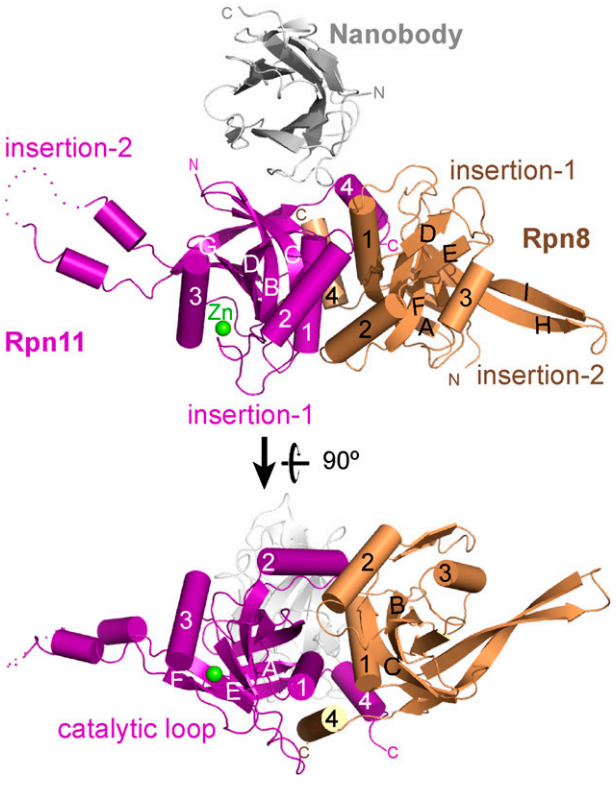

Fig. 2. Crystal structure of the MPN domain fusion protein of Rpn8 and Rpn11 with the attached nanobody. The composite structure of Rpn8 (chain A) from crystal form II superposed on the Rpn8-Rpn11–nanobody complex (chains D, E, and F) from crystal form Ia is shown in side and bottom views. The Rpn8 and Rpn11 units are indicated in purple and brown, respectively; the nanobody is represented in silver. Disordered segments are indicated by dotted lines. Helices are represented by cylinders; the catalytic Zn ion, by a green sphere. The unique insertions into the canonical MPN structure are indicated.

Role of the Nanobody in Crystal Formation. The nanobody contacts an area that involves β-strands βB, βC, and βG and α4 in Rpn11 and a section of helix α1 in Rpn8, thereby establishing additional contacts between the proteins and rigidifying the complex (Fig. 2). This contact area forms a depression on the surface of the Rpn8-Rpn11 complex, providing a concave binding site for the CDR3 loop of the nanobody. Furthermore, in all crystal lattices, the nanobodies contribute important crystal contacts to adjacent Rpn8 molecules. Thus, a combination of both effects might explain why the nanobody is required for the successful crystallization of Rpn8-Rpn11.

Active Site of Rpn11. The active site of MPN domain metalloproteases is located between the N-terminal end of helix α3 and the adjacent β-strands βB and βD (31, 33, 34). Clear density for the catalytic zinc was identified between the sidechains of His109, His111, and Asp122 (Fig. 3*A* and Fig. S4*A*). These sidechains, together with a water molecule, form a slightly distorted tetrahedral coordination shell around the metal ion. This core structure is almost identical to that of the DUB AMSH-LP (25, 33, 34), for which both apo and substrate-bound crystal structures have been characterized at high-resolution (Fig. 3*B* and Fig. S4*E*). In the AMSH-LP cocrystal structure, the isopeptide bond carbonyl group was positioned directly on top of the metal site (Fig. 3*B*) (34), strongly suggesting that this conformation of Rpn8-Rpn11 represents a catalytically active state.

The residue Glu48 at the beginning of β-strand βB corresponds to residue Glu292 of AMSH-LP, which is essential for AMSH-LP activity (25, 33). Mutating this residue to glutamine abolished Ub_4 cleavage activity in Rpn8-Rpn11 (Fig. 1*B*). Glu48 is positioned for activation of the attacking water molecule and protonation of the isopeptide amide group. With the location of Glu48, His109, and His111 in two adjacent β-strands, the respective geometry is largely fixed (Fig. 3*A* and Fig. S4*A*). The conformation of the catalytic loop (residues 109–122) is stabilized by an extended hydrogen bond network in Rpn11 (Fig. 3*A* and Fig. S4*A*), which is also observed in the apo crystal structures of AMSH-LP (25), the Rpn11 paralog Csn5 (31), and the archaeal Rpn11 homolog AfJAMM (24) (Fig. S4 *D*–*F*). Hydrogen bond contacts between the carbonyl group of Gly115 and the imidazole ring of His111 and between the amide group of Ser119 and the carboxyl group of Asp122 orient the coordinating sidechains toward Zn and establish the proper polarity. The imidazole ring of His111 is further buttressed by the sidechains of the catalytic loop residues Phe114 and Trp117 (Fig. 3*A* and Fig. S4*A*). The orientation of the indole group of Trp117 is stabilized by a hydrogen bond to the carbonyl group of Phe114. In addition, the carboxyl group of Asp142 links the amide groups of Gly115 and Ile144. These two interactions are conserved in Csn5 as well (31, 32) (Fig. S4*F*). Asp142 and Ile144 belong to the highly conserved loop connection between βE and βF in Rpn11. The respective loop is much shorter in AMSH-LP. Other important hydrogen bond contacts with the backbone are formed by the JAMM motif residues Ser110 and Ser119. The former extends the β-sheet contacts between βB and βD, and the latter stabilizes the N-terminal part of helix α3 and buttresses Asp122.

Alternative conformations of the catalytic loop were found in one of the two copies of Rpn11 in crystal forms Ia and Ib each (Fig. 3*C* and Fig. S4 *B* and *C*). Both conformers are characterized by a wider separation of the His111 imidazole ring from Zn (2.9 Å vs. 2.1 Å), whereas His109 and Asp122 remain virtually

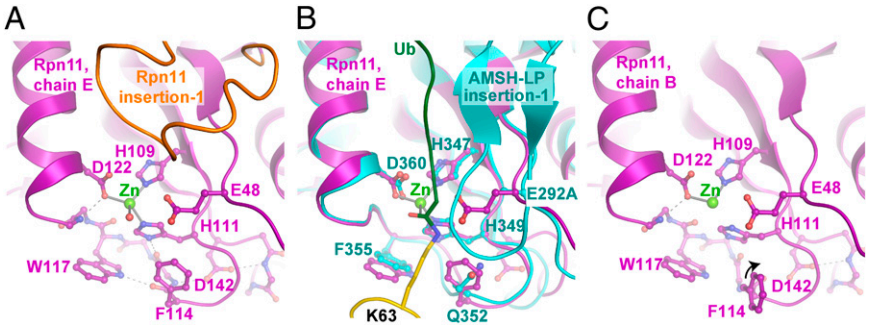

Fig. 3. Active site of Rpn11. (*A*) Detailed view of the Rpn11 active site. The catalytic residues are shown in ball-and-stick representation. Hydrogen bonds are indicated by dashed lines. This represents the active conformation found in complex DEF of crystal form Ia. Insertion 1 in Rpn11 is highlighted in orange. (*B*) Superposition with the AMSH-LP-Ub_2 complex showing the likely orientation of the isopeptide bond in the substrate complex. AMSH-LP, the proximal and distal Ub are shown in cyan, gold, and green, respectively. Insertion 1 of Rpn11 has been removed for clarity. (*C*) Distorted active site geometry in complex ABC of crystal form Ia.

unchanged. This rearrangement should alter the properties of the Zn ion and thereby decrease catalytic activity. The expected water ligands bound to Zn are poorly defined in these conformations and are not included in the model. The reorientation of the His111 sidechain largely disrupts the hydrogen bond network of the catalytic loop. Thus, this mechanism may render the catalytic center geometry sensitive to local changes. In the crystal lattice, the active conformation likely is stabilized by a crystal contact with the sidechain of Phe114. In the context of the 26S proteasome, the adjacent highly conserved loop connection between βE and βF is a good candidate for the regulation of activity; it is in contact with helix α4 of Rpn8, and its conformation is likely to be sensitive to rearrangements in the RP.

Ub Binding. Superposition with the AMSH-LP-Ub_2 structure suggests that the binding site for the substrate-ligated Ub moiety is located in the shallow groove between helices α2 and α3 of Rpn11 (Fig. 3*B*). Compared with AMSH-LP, helix α2 is differently oriented in Rpn11 (Fig. 4*A*). This orientation is enforced by conserved hydrophobic interactions with the α2 helix of Rpn8 in the Rpn8-Rpn11 complex (Fig. 4*B*). Thus, a reorientation to the conformation observed in AMSH-LP seems improbable.

The putative Ub-binding site is largely hydrophobic in character, with the notable exception of Asp85, which is replaced by Pro in the majority of Rpn11 sequences (Fig. 4*C*). The highly conserved Asp84 might functionally replace AMSH-LP residue Glu329, which contacts Lys48 of the distal Ub. The other key contact residues in AMSH-LP, Val328, Phe332, Thr342, and Met370, are replaced by Val86, Ala89, Val104, and Leu132, respectively, in Rpn11. The putative Ub-contacting Rpn11 residues Asp85, Val86, Gln88, Ala89, Met92, Met103, Val104, Ser128, Gln131, Leu132, and Asn133 are less conserved compared with the residues facing other subunits of the RP, suggesting evolutionary pressure against high-affinity binding at this site in Rpn11 (see below) (Fig. 4*B*). Only charged residues seem to be forbidden in the Ub contact area.

In the AMSH-LP-Ub_2 structure, the C terminus of the distal Ub aligns with helix α3 and forms β-contacts with insertion 1, which assumes a β-hairpin conformation (Fig. 3*B*). The contact residues in helix α3 are conserved between AMSH-LP and Rpn11. Insertion 1 of AMSH-LP also forms a β-hairpin conformation in the absence of Ub (25). In the Rpn8-Rpn11 structures, insertion 1 forms a loop structure including a helical turn, which blocks the path of the Ub C terminus (Fig. 3*A*). The loop conformation, which is stabilized by hydrogen bonds between the hydroxyl group of Ser79 with the amide of Glu81 and the carbonyl of Thr76, is rather poorly defined in the structures. It makes few van der Waals contacts to the remainder of Rpn11, suggesting considerable structural plasticity. Moreover, the loop has the same length and a similar polarity pattern in AMSH-LP and Rpn11. Glu81 in Rpn11 replaces Asp324 in AMSH-LP, which forms an electrostatic interaction with Arg74 of Ub. Thus, remodeling to a conformation similar to that of AMSH-LP seems possible in Rpn11. Regulated rearrangement of this highly conserved segment in the context of the RP might provide another layer of control against premature Rpn11 activation.

Contacts of Rpn8-Rpn11 in the 26S Proteasome. We next fitted the Rpn8-Rpn11 core complex crystal structure into the EM densities of the *S. cerevisiae* 26S proteasome in the substrate-accepting (13) and the substrate-engaged states (27) (Fig. 5 *A* and *B*). The resolved secondary structure elements of both maps are in excellent agreement, with the notable exception of insertion 2 of Rpn11, which also varies significantly in the different crystal forms (Fig. S2*D*). Thus, the structure of the Rpn8-Rpn11 core complex in isolation is indistinguishable from that in the different 26S conformers at the level of resolution of the cryo-EM maps (Fig. 5 *A* and *B*). Nb1 would severely clash with Rpn2 helices H28 and H30 in both proteasomal conformations

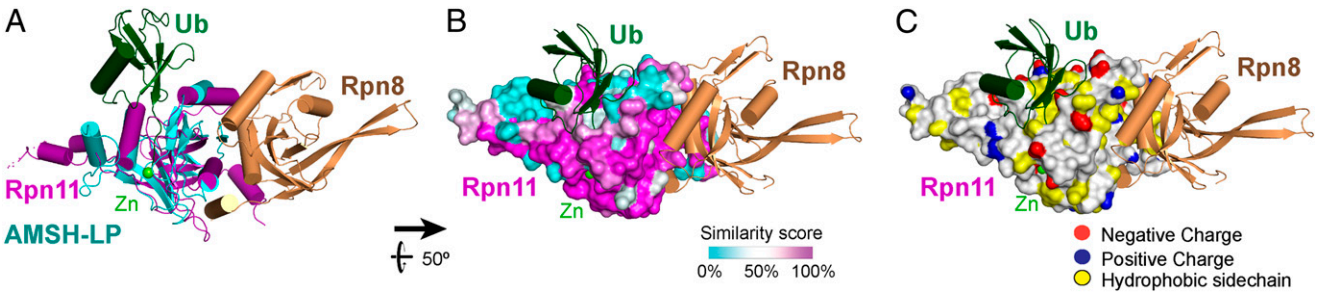

Fig. 4. Binding site for the proximal Ub. (*A*) Superposition of Rpn11 with the AMSH-LP-Ub_2 complex. AMSH-LP and the distal Ub are shown in cyan and green, respectively. (*B*) Surface conservation at the Rpn11 Ub-binding site. The similarity score from the sequence alignment shown in Fig. S3 was mapped onto the surface of Rpn11. A magenta-white-cyan color gradient represents decreasing surface conservation. (*C*) Surface view of Rpn11 showing the residue properties at the putative Ub-binding site. Hydrophobic sidechains are highlighted in yellow; positive and negative charged groups are shown in blue and red, respectively.

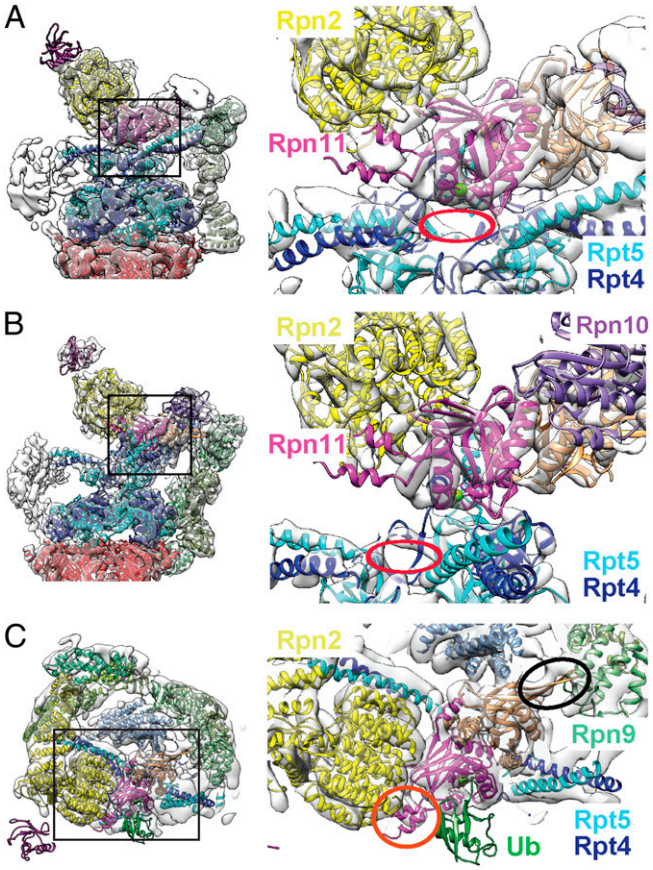

Fig. 5. Docking of the Rpn8-Rpn11 MPN domain complex into 26S proteasome EM density. (*A* and *B*) Rpn8-Rpn11 MPN domain dimer docked into the cryo-EM density of the substrate-engaged and -accepting states of the 26S proteasome, respectively. The green sphere represents the active site zinc ion. The red ring indicates the AAA ATPase pore entrance. Contacting subunits to Rpn8-Rpn11 are indicated. (*C*) Top view of the substrate-engaged state. Insertion 2 of Rpn8 fits into density bridging the gap toward the PCI horseshoe complex at subunit Rpn9 (circled in black). Insertion 2 of Rpn11 fits into an unassigned density close to the PC domain of Rpn2 (circled in orange).

(see Fig. S6 *A* and *B*), suggesting that its inhibitory effect may be related to a perturbation of the holocomplex. In fact, addition of the nanobody to purified 26S proteasomes appeared to largely disrupt the particles, as observed in cryo-EM.

In both 26S states, the MPN domain of Rpn11 makes extensive contacts with the central torus-shaped domain of Rpn2 on one side and the coiled-coil extensions of Rpt3, Rpt4, and Rpt5 and the OB domains of Rpt4 on the other side. The contact areas are highly conserved in Rpn11 and its binding partners (Figs. S5 *A–D* and S6 *C* and *D*). The interface with Rpn2 likely involves Rpn11 βA, the βB-βC hairpin, and insertion 2, all of which appear to be flexible in the crystal structures. A flexibly attached, highly conserved segment is found at the tip of insertion 2 in Rpn11, residues 169–178 (EPRQTTSNTG) (Fig. S3), which might insert into a conspicuously conserved groove between helices H20 and H22 on the outer surface of the Rpn2 torus (Fig. S6*A*). Between this patch and the MPN domain proper, an as-yet unassigned density was observed that likely corresponds to the Rpn11 insertion 2 helices and possibly also the N-terminal 22 residues of Rpn11 that are disordered in all crystallographic models. This density appears to be best resolved for the GFP substrate-bound 26S proteasome structure (26).

The contacts to the ATPases involve the catalytic loop, insertion 1, and the βE-βF connecting loop, which are important for substrate access and Rpn11 active site geometry, and the link between α1 and βB. During the transition from the substrate-accepting to the substrate-engaged state, the Rpt4-Rpt5 coiled coil slides away from insertion 1, perhaps stabilizing the insertion 1 on substrate isopeptide link intrusion. The N-terminal end of the Rpt3 coiled coil buttresses the βE-βF loop, and the OB domain of Rpt4 moves in close vicinity to the catalytic loop, presumably stabilizing its active conformation. The C terminus of the docked Ub moiety would be surrounded by protein in the substrate-engaged state.

Insertion 2 of Rpn8 reaches toward the solenoid segment of the PCI domain subunit Rpn9 (Fig. 5*C*). Density for this connection is clearly discernible in the cryo-EM maps. Apart from this interaction, the MPN domain of Rpn8 serves as attachment site for the von Willebrand (VWA) domain of Rpn10 together with Rpn9 (Figs. S5 and S6 *A* and *B*). The Rpn10 contact region, largely identical to insertion 1, represents the most highly conserved surface region within Rpn8 on the Rpn8-Rpn11 complex (Fig. S5 *A* and *B*). In the 26S holocomplex, Rpn10 is situated next to the exposed binding site for the substrate-ligated Ub and might engage in additional contacts with the polyubiquitin chain. A Lys48-linked Ub would be in close contact with the VWA domain of Rpn10 and the N-terminal part of the Rpt4-Rpt5 coiled-coil bundle (35). Further Lys-48–linked Ub moieties could be bound by the C-terminal Ub-interaction motifs (UIMs) in Rpn10 in the committed proteasome (Fig. 6) (36).

Regulation of Rpn11 Activity in the 26 Proteasome. Through the analysis of fusion protein crystal structures, we have identified three potential mechanisms for preventing premature activation of the isopeptidase activity of Rpn11: (*i*) establishment of the correct active site geometry, (*ii*) rearrangement of Rpn11 insertion 1 to allow access of the proximal Ub C terminus to the catalytic site, and (*iii*) low affinity of the proximal Ub to its docking site on Rpn11. The basal isopeptidase activity of the Rpn8-Rpn11 fusion protein indicates that in principle, all of these obstacles can be overcome outside of the 26S proteasome, albeit with low efficiency. The Rpn8-Rpn11 conformers in the

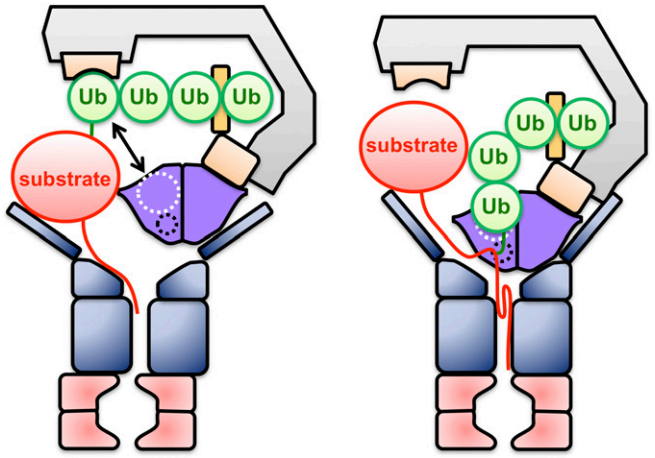

Fig. 6. Schematic model for 26S proteasome isopeptide bond cleavage. Models for the substrate-accepting and -engaged state of the proteasome are shown. Folded and extended parts of the substrate are indicated by red spheres and red lines, respectively. Poly-Ub–tagged substrate proteins are recognized by the Ub receptors Rpn13 and Rpn10 (pale yellow) and Rpn10 UIM (yellow). Rpn11 reaches the isopeptide bond only when the substrate is already partially unfolded (Rpn8-Rpn11; purple). The white and black dashed circles designate the primary Ub-binding site and active site of Rpn11, respectively.

crystal structures show that proper active site geometry is accessible, but not stable. Similarly, insertion 1 of Rpn11 blocks the access path for Ub in our structures; however, this element appears to be mobile, as suggested by the high B-factors and disorder in several conformers, and thus it should rearrange easily once the Ub C terminus enters the access path.

The affinity of the Rpn8-Rpn11 fusion protein for Ub appears to be modest at best (Fig. 1*B*). Simultaneous contacts with both sites should allow efficient substrate binding only in the close presence of Ub receptors, particularly the Rpn10 UIM motif, in the assembled proteasome. In support of this idea, a 26S complex without Rpn10 and Rpn13 demonstrated greatly reduced Ub_4 cleavage activity (Fig. S8). Another mechanism of preventing cleavage of noncommitted substrates is limited access for bulky folded domains to the narrow surroundings of the Rpn11 active site in both 26S conformations.

Full activation of Rpn11 is presumably realized by contacts with the coiled coils and the OB ring of the AAA subunits, which have been proposed to have chaperone activity (37) and furthermore could stabilize the active conformation in Rpn11 and thereby increase the affinity for the primary Ub by opening the binding site for the C-terminal tail. The strong sequence conservation of the involved elements suggests tight coevolution of a defined functional interface (Figs. S5 *A–D* and S6 *C* and *D*). Therefore, the 26S proteasome might have an extended "composite" deubiquitylase active site, converting the access groove for the C-terminal end of the Ub chain in AMSH-LP into a channel, which allows exact control of substrate orientation; this is necessary because the sequences flanking Ub acceptor sites are variable in proteasomal substrates. Only the structure of polyubiquitylated substrate bound to Rpn11 in the context of a stalled proteasome will reveal the molecular mechanism of deubiquitylation in full detail.

Materials and Methods

The experimental procedures are described in detail in *SI Materials and Methods*. In brief, Rpn8-Rpn11 from *S. cerevisiae* was expressed as a His6 tag fusion protein including a tobacco etch virus (TEV) protease site in *E. coli* BL21 (DE3) cells and purified by Ni-affinity chromatography, TEV cleavage, and Superose-12 size exclusion chromatography. Crystals were grown using 50 mM MES pH 6.0, 200 mM Ca acetate, and 22% (wt/vol) PEG-3350 or with 50 mM MES pH 6.0, 100 mM $MgCl_2$, and 21% (wt/vol) PEG-3350. The Rpn8-Rpn11-nanobody crystal structure was solved by molecular replacement. The isopeptidase activity assay was performed with a fluorogenic Ub_4 fusion protein, with reaction progress monitored by fluorescence polarization. The nanobody was selected and produced following standard procedures (38).

ACKNOWLEDGMENTS. We thank Yousuf Mohiuddin Mohammed, André Mourão, Günter Pfeifer, Oana Mihalache, Sándor Varga, Ágnes Hubert, Jan Schuller, Antje Aufderheide, Andreas Schweitzer, Pia Unverdorben, and Roman Körner (Max Planck Insitute of Biochemistry); Alison Lundquist (Vrije Universiteit Brussels); Ethan Emberley, Brajesh Kumar, and David J. Wustrow (Cleave Biosciences); the Joint Structural Biology Group group at the Electron Synchrotron Radiation Facility Grenoble; and staff at Swiss Light Source X10SA Villigen, the MPIB Crystallization Facility, and the MPIB Core Facility for their excellent support. Our research is supported by funding from the Deutsche Forschungsgemeinschaft Excellence Cluster Center for Integrated Protein Science Munich and SFB-1035/Project A01 (to W.B.), Instruct (part of the European Strategy Forum on Research Infrastructures and supported by national member subscriptions) through a Research and Development Pilot Project grant (to J.S., I.N., and P.Ś.), as well as Graduiertenkolleg 1721 (to F.F.) and European Molecular Biology Organization (to P.Ś.).

1. Finley D (2009) Recognition and processing of ubiquitin-protein conjugates by the proteasome. *Annu Rev Biochem* 78:477–513.
2. Goldberg AL (2003) Protein degradation and protection against misfolded or damaged proteins. *Nature* 426(6968):895–899.
3. Varshavsky A (2012) The ubiquitin system, an immense realm. *Annu Rev Biochem* 81:167–176.
4. Buchberger A, Bukau B, Sommer T (2010) Protein quality control in the cytosol and the endoplasmic reticulum: Brothers in arms. *Mol Cell* 40(2):238–252.
5. Hershko A, Ciechanover A, Varshavsky A (2000) Basic Medical Research Award: The ubiquitin system. *Nat Med* 6(10):1073–1081.
6. Tanaka K (2009) The proteasome: Overview of structure and functions. *Proc Jpn Acad, Ser B, Phys Biol Sci* 85(1):12–36.
7. Voges D, Zwickl P, Baumeister W (1999) The 26S proteasome: A molecular machine designed for controlled proteolysis. *Annu Rev Biochem* 68:1015–1068.
8. Förster F, Unverdorben P, Sledź P, Baumeister W (2013) Unveiling the long-held secrets of the 26S proteasome. *Structure* 21(9):1551–1562.
9. Baumeister W, Walz J, Zühl F, Seemüller E (1998) The proteasome: Paradigm of a self-compartmentalizing protease. *Cell* 92(3):367–380.
10. Peters JM, Cejka Z, Harris JR, Kleinschmidt JA, Baumeister W (1993) Structural features of the 26 S proteasome complex. *J Mol Biol* 234(4):932–937.
11. Lasker K, et al. (2012) Molecular architecture of the 26S proteasome holocomplex determined by an integrative approach. *Proc Natl Acad Sci USA* 109(5):1380–1387.
12. Lander GC, et al. (2012) Complete subunit architecture of the proteasome regulatory particle. *Nature* 482(7384):186–191.
13. Beck F, et al. (2012) Near-atomic resolution structural model of the yeast 26S proteasome. *Proc Natl Acad Sci USA* 109(37):14870–14875.
14. Glickman MH, et al. (1998) A subcomplex of the proteasome regulatory particle required for ubiquitin-conjugate degradation and related to the COP9-signalosome and eIF3. *Cell* 94(5):615–623.
15. Śledź P, et al. (2013) Structure of the 26S proteasome with ATP-γS bound provides insights into the mechanism of nucleotide-dependent substrate translocation. *Proc Natl Acad Sci USA* 110(18):7264–7269.
16. Beckwith R, Estrin E, Worden EJ, Martin A (2013) Reconstitution of the 26S proteasome reveals functional asymmetries in its AAA+ unfoldase. *Nat Struct Mol Biol* 20(10):1164–1172.
17. Pathare GR, et al. (2012) The proteasomal subunit Rpn6 is a molecular clamp holding the core and regulatory subcomplexes together. *Proc Natl Acad Sci USA* 109(1):149–154.
18. Estrin E, Lopez-Blanco JR, Chacón P, Martin A (2013) Formation of an intricate helical bundle dictates the assembly of the 26S proteasome lid. *Structure* 21(9):1624–1635.
19. Enchev RI, Schreiber A, Beuron F, Morris EP (2010) Structural insights into the COP9 signalosome and its common architecture with the 26S proteasome lid and eIF3. *Structure* 18(4):518–527.
20. Sun C, et al. (2011) Functional reconstitution of human eukaryotic translation initiation factor 3 (eIF3). *Proc Natl Acad Sci USA* 108(51):20473–20478.
21. Querol-Audi J, et al. (2013) Architecture of human translation initiation factor 3. *Structure* 21(6):920–928.
22. Yao T, Cohen RE (2002) A cryptic protease couples deubiquitination and degradation by the proteasome. *Nature* 419(6905):403–407.
23. Verma R, et al. (2002) Role of Rpn11 metalloprotease in deubiquitination and degradation by the 26S proteasome. *Science* 298(5593):611–615.
24. Ambroggio XI, Rees DC, Deshaies RJ (2004) JAMM: A metalloprotease-like zinc site in the proteasome and signalosome. *PLoS Biol* 2(1):E2.
25. Sato Y, et al. (2008) Structural basis for specific cleavage of Lys 63-linked polyubiquitin chains. *Nature* 455(7211):358–362.
26. Matyskiela ME, Lander GC, Martin A (2013) Conformational switching of the 26S proteasome enables substrate degradation. *Nat Struct Mol Biol* 20(7):781–788.
27. Gallery M, et al. (2007) The JAMM motif of human deubiquitinase Poh1 is essential for cell viability. *Mol Cancer Ther* 6(1):262–268.
28. Bivona TG, et al. (2011) FAS and NF-κB signalling modulate dependence of lung cancers on mutant EGFR. *Nature* 471(7339):523–526.
29. Spataro V, Simmen K, Realini CA (2002) The essential 26S proteasome subunit Rpn11 confers multidrug resistance to mammalian cells. *Anticancer Res* 22(6C):3905–3909.
30. Sanches M, Alves BS, Zanchin NI, Guimarães BG (2007) The crystal structure of the human Mov34 MPN domain reveals a metal-free dimer. *J Mol Biol* 370(5):846–855.
31. Echalier A, et al. (2013) Insights into the regulation of the human COP9 signalosome catalytic subunit, CSN5/Jab1. *Proc Natl Acad Sci USA* 110(4):1273–1278.
32. Zhang H, et al. (2012) The crystal structure of the MPN domain from the COP9 signalosome subunit CSN6. *FEBS Lett* 586(8):1147–1153.
33. Davies CW, Paul LN, Kim MI, Das C (2011) Structural and thermodynamic comparison of the catalytic domain of AMSH and AMSH-LP: Nearly identical fold but different stability. *J Mol Biol* 413(2):416–429.
34. Kikuchi K, Ishii N, Asao H, Sugamura K (2003) Identification of AMSH-LP containing a Jab1/MPN domain metalloenzyme motif. *Biochem Biophys Res Commun* 306(3):637–643.
35. Rani N, Aichem A, Schmidtke G, Kreft SG, Groettrup M (2012) FAT10 and NUB1L bind to the VWA domain of Rpn10 and Rpn1 to enable proteasome-mediated proteolysis. *Nat Commun* 3:749.
36. Riedinger C, et al. (2010) Structure of Rpn10 and its interactions with polyubiquitin chains and the proteasome subunit Rpn12. *J Biol Chem* 285(44):33992–34003.
37. Djuranovic S, et al. (2009) Structure and activity of the N-terminal substrate recognition domains in proteasomal ATPases. *Mol Cell* 34(5):580–590.
38. Pardon E, et al. (2014) A general protocol for the generation of nanobodies for structural biology. *Nat Protoc*, in press.